Comprehensive Study of Switching Overvoltages in Transmission Line of Northern Laos Power Grid Interconnected Across Pakbeng–Tha Wang Pha Region

Ketsaphone Phandolak,
Kanchit Ngamsanroaj, and **Watcharin Srirattanawichaikul**†, Non-members

ABSTRACT

Switching and temporary overvoltages pose critical challenges to the reliable operation of extra-high-voltage (EHV) transmission networks. This study analyzes the 500 kV Pakbeng–Tha Wang Pha (PKB–TWP) cross-border interconnection between Laos and Thailand, an essential corridor for regional hydropower integration. A probabilistic electromagnetic transient model was developed in PSCAD/EMTDC to evaluate switching overvoltages and temporary overvoltages under realistic operating conditions. Monte Carlo simulations incorporating Gaussian breaker-pole scatter and representative temporary overvoltage scenarios—such as the Ferranti effect, load rejection, and transformer inrush—were performed. Uncontrolled line energization produced surges up to 2.251 p.u., while reclosing after three-phase-to-ground faults reached 3.445 p.u., both exceeding the ≈ 2.0 p.u. insulation coordination threshold. The use of 444 kV metal-oxide surge arresters and 110 Mvar shunt reactors together brought all surges below 2.0 p.u., meeting the IEC 60071-2 withstand requirements. Temporary overvoltages were contained within an acceptable level: 1.157 p.u. (Ferranti effect), 1.317 p.u. (90% load rejection), and 1.71 p.u. (transformer inrush). Spatial analysis identified resonance hotspots near midline sections, emphasizing the importance of distributed monitoring. Overall, the PKB–TWP interconnection was verified to be technically robust, and the proposed methodology provides a practical framework for future EHV insulation coordination in Southeast Asia.

Keywords: Switching overvoltage, Temporary overvoltage, Insulation coordination, 500 kV Transmission line, PSCAD/EMTDC

1. INTRODUCTION

High-voltage transmission systems are vulnerable to transient overvoltages, particularly those caused by switching operations and operational disturbances. These overvoltages, if not adequately mitigated, can compromise insulation strength, accelerate equipment aging, and in extreme cases threaten system security. In extra- and ultra-high-voltage networks, switching overvoltages and temporary overvoltages are of particular concern because they are influenced by line resonance, weak-grid interactions, and transformer energization phenomena [1].

In Southeast Asia, the rapid development of regional power exchange has heightened the importance of robust insulation coordination. The 500 kV PKB–TWP transmission corridor, spanning approximately 120 km, plays a critical role in delivering hydropower from Laos to the Thailand power grid. However, the project faces several technical challenges, including long line lengths that amplify the Ferranti effect, weak short-circuit strength at the receiving end, and frequent reclosings due to lightning strikes in the region. The Nam Theun 2–Roi Et 2 interconnection has shown that energization without protection can cause surges exceeding 2.0 p.u., which exceed insulation capability [2], [3]. Previous work [4] developed a simplified arc model for evaluating single-phase reclosing in 500 kV systems, which provided the basis for extending this overvoltage study to transient phenomena.

Recent studies emphasize probabilistic approaches over traditional deterministic methods for assessing switching surges. Deterministic methods rely on fixed breaker-closing angles and often underestimate the stochastic variation observed in practice [4], [5]. In contrast, probabilistic Monte Carlo simulations capture variability in pole scatter and yield realistic probability envelopes, making them widely adopted in UHV studies [5]–[6]. At the same time, temporary overvoltages arising from the Ferranti effect, load rejection, and transformer inrush continue to pose significant challenges for 500 kV-class interconnections [1], [7].

This paper investigates the switching and temporary overvoltage performance of the 500-kV PKB-TWP transmission system using a probabilistic electromagnetic

Manuscript received on October 10, 2025; revised on December 4, 2025; accepted on December 31, 2025. This paper was recommended by Associate Editor Vuttipon Tarateeraseth.

The authors are with Department of Electrical Engineering, Faculty of Engineering, Chiang Mai University, Chiang Mai, Thailand.

†Corresponding author: watcharin.s@cmu.ac.th

Digital Object Identifier: 10.37936/ecti-eec.2026241.261810

transient simulation framework. The key contributions of this study are summarized as follows:

- A detailed dynamic modeling approach is developed, incorporating frequency-dependent phase-domain line modeling and nonlinear representations of transformers, generators, shunt reactors, surge arresters, and circuit breakers to capture both fast-front and slow-front overvoltages accurately.
- A statistical switching mechanism is introduced by modeling circuit-breaker pole scatter as a Gaussian random variable, enabling realistic estimation of switching-surge variability under practical operating conditions.
- A Monte Carlo Simulation framework is formulated to obtain percentile-based overvoltage indices (95th and 98th percentiles) in accordance with IEC 60071-2, providing a probability-based insulation coordination methodology for EHV systems.
- Comprehensive analysis is performed for multiple operating scenarios, including line energization, reclosing, load rejection, transformer energization, and long-line Ferranti effects within the Laos–Thailand 500-kV corridor.

The structure of this paper is organized as follows. Section 2 presents the dynamic EMT modeling approach and probabilistic switching methodology. Section 3 provides the problem formulation, component modeling, and Monte Carlo evaluation process. Section 4 discusses the results of switching and temporary overvoltages under various operational scenarios, which present engineering implications and reliability considerations. Finally, Section 5 concludes the major findings of this study.

2. SYSTEM DESCRIPTION

Fig. 1 illustrates the transmission system analyzed in this study, based on the planned 500 kV PKB–TWP double-circuit interconnection linking the Lao PDR power grid and Thailand's national power system. The sending end comprises 14 generators totaling 57 MVA and 11 kV hydro generators, for a total generation capacity of 798 MVA. Each generator is connected to a 63.3-MVA, 525/11-kV step-up transformer, resulting in an overall capacity of 886.2 MVA. To improve voltage stability and mitigate the Ferranti effect, the 500 kV bus is equipped with three 55 Mvar shunt reactors. An additional 444 kV metal-oxide surge arrester is installed to protect against switching surges and temporary overvoltages.

The surge-arrester rating complies with IEC 60099-4 and the manufacturer's protective data (ABB HS PEXLim P-T), with a continuous operating voltage of 354 kVrms (289 kV L–G), ensuring an adequate protection margin for temporary overvoltages up to 1.5 p.u. and maintaining a residual voltage below 1.1 MV at 10 kA. The arrester is classified as IEC Class 4, with a nominal discharge current of 20 kA and a 4/10-μs high-current withstand capability of 100 kA [17], [18]. At the receiving end, a 110-Mvar shunt reactor is installed to compensate approximately 70–80% of the reactive power produced by the 120-km double-circuit transmission line.

In PSCAD/EMTDC, the sending-end hydro generators are modeled as equivalent AC voltage sources, with Thevenin impedances derived from a short-circuit capacity of 8,021 MVA. Governor and excitation-system dynamics are neglected because they have minimal influence on high-frequency electromagnetic transients.

The interconnection is modeled as a 120-km, double-circuit transmission line in PSCAD/EMTDC, using the frequency-dependent phase-domain model to simulate the behavior of transient electromagnetic waves accurately. Each circuit uses 795 MCM quad-bundle ACSR conductors, consistent with the regional 500 kV transmission design standard. To assess spatial variations in overvoltage phenomena, the line is segmented into four 30-km sections, with monitoring nodes placed at each boundary. At the receiving end, the Thailand power grid is represented by a 500 kV infinite bus, including equivalent surge arresters and aggregated load models. All parameters comply with the project's design specifications and the IEC 60071 insulation coordination guidelines.

The short-circuit levels at both ends of the 500 kV PKB–TWP interconnection were derived from the transmission system planning data. The sending-end bus PKB has a three-phase short-circuit capacity of 8,021 MVA ($\approx$ 9.26 kA at 500 kV), representing a strong hydro generation source. The receiving-end bus TWP has a short-circuit capacity of 10,728 MVA ($\approx$ 12.39 kA), corresponding to the interconnection with Thailand's national power grid. These short-circuit capacities were implemented in PSCAD/EMTDC as Thevenin equivalents to accurately represent system strength and ensure realistic simulation of switching and temporary overvoltages.

Similar 500 kV transmission corridors, such as the Nam Theun 2–Roi Et 2 interconnection, have demonstrated transient behavior comparable to that during energization and reclosing events, confirming the validity of the modeling approach adopted in this study.

As illustrated in Fig. 1, the system comprises the sending-end hydro generators and step-up transformers, three 55 Mvar shunt reactors, and a 120 km double-circuit 500 kV transmission line divided into 70 km and 50 km sections. The receiving-end bus at Tha Wang Pha includes two 750 MVA equivalent sources and 110 Mvar shunt reactors for voltage support. This configuration represents the complete layout, modeled in PSCAD/EMTDC, for electromagnetic transient analysis.

Switching and temporary overvoltages represent major operational challenges in long extra-high-voltage transmission systems. Switching overvoltages occur during line energization, reclosing, or fault recovery and can exceed insulation coordination limits if not ade-

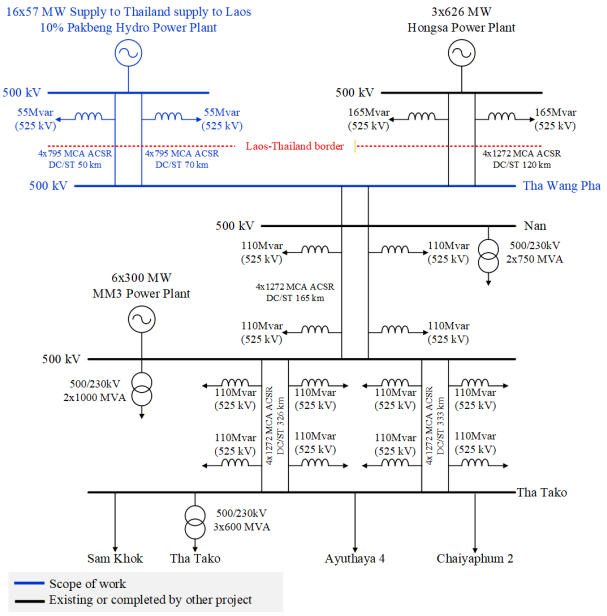

***Fig. 1**: Single-line diagram of the 500 kV PKB–TWP.*

quately mitigated. These surges are particularly severe under light- or no-load conditions, where line-charging capacitance dominates the transient response. Similarly, temporary overvoltages arise from steady-state or slow transients such as the Ferranti effect, load rejection, and transformer inrush, which may sustain elevated voltage stresses for several cycles and compromise insulation [10]–[12].

For the 500-kV PKB–TWP interconnection, the 120-km double-circuit configuration and relatively low short-circuit strength at the receiving end increase its susceptibility to both switching-overvoltage and temporary-overvoltage events. Although shunt reactors and metal-oxide surge arresters are standard mitigation measures in EHV systems [9], their coordinated performance under multiple operating scenarios has not yet been comprehensively validated for this corridor.

Previous studies on comparable 500 kV interconnections—such as the Nam Theun 2–Roi Et 2 project—have shown that uncompensated or improperly tuned systems may experience switching surges exceeding 2.0 p.u., surpassing insulation withstand levels [2], [3]. However, no detailed electromagnetic transient (EMT) analysis of the PKB–TWP system has been reported to date. The present study addresses this gap by performing full EMT-based simulations to evaluate switching and temporary overvoltages under realistic operating conditions, ensuring compliance with IEC 60071-2 insulation coordination requirements and supporting the design of a robust and reliable 500 kV cross-border interconnection.

3. THEORY AND METHODOLOGY

3.1 Switching overvoltages in power systems

Switching and temporary overvoltages are dominant transient phenomena in extra-high-voltage networks and

***Table 1**: Summary of test system parameters for the 500 kV PKB–TWP Interconnection.*

Component	Substation	Rating	Description
Generator	PKB Hydropower Plant	14 × 57 MVA, 11 kV	Synchronous hydro units; total capacity = 798 MVA
Step-up Transformer	PKB	63.3 MVA, 525/11 kV, Δ–Yd1	Connect each generator to the 500 kV bus
Transmission Line	PKB – TWP corridor	500 kV, 120 km (double circuit), 795 MCM quad-bundle ACSR	Frequency-dependent phase-domain model; 30 km per section
Shunt Reactor	PKB	3 × 55 Mvar at 500 kV	Mitigates the Ferranti effect during no-load operation
	TWP	2 × 110 Mvar at 500 kV	Provides voltage support and reactive compensation
Surge Arrester (MOSA)	PKB/TWP	444 kV rated voltage; Uc = 354 kVrms (L–L); IEC 60099-4 Class 4	Protects against switching and temporary overvoltages
Auto-Transformer	TWP	2 × 750 MVA, 525/242 kV, Yy0,d1 connection	Interfaces the Lao 500 kV system with the Thai grid
Equivalent Source	PKB (bus)	Short-circuit capacity = 8,021 MVA (≈ 9.26 kA at 500 kV)	Represents hydro generation strength
	TWP (bus)	Short-circuit capacity = 10,728 MVA (≈ 12.39 kA at 500 kV)	Represents the Thailand national grid strength
Source Impedance	TWP (230 kV level)	$R_1 = R_2 =$ 0.00509 p.u.; $X_1 = X_2 =$ 0.04645 p.u.	Equivalent Thevenin model for EMT simulation
Circuit Breaker	PKB / TWP	LTB 550 E2, 550 kV, 50 kA, ABB type	For energization and reclosing studies

arise from the nonlinear interaction of transmission lines, transformers, shunt reactors, surge arresters, and circuit breakers. Their theoretical modeling is fundamental for evaluating the insulation performance of the 500-kV PKB–TWP interconnection [3], [5], [20].

Switching overvoltages occur during line energization, re-energization, capacitor or inductor switching, and fault initiation or clearing [1], [4]. For line energization, the network's transient behavior can be represented by a series RLC circuit driven by an applied voltage [13].

$$V_s(t) = V_s \sin(\omega t + \delta T) \tag{1}$$

where V_s is the source voltage magnitude, ω is the angular frequency of the system, and δT represents the

breaker pole-closing angle deviation.

The resulting electrical response produces damped oscillatory surges typically between 2.4 and 2.8 p.u., whereas re-energization may reach 3.5–4.0 p.u. due to trapped charge [6]. Fault-clearing produces transient recovery voltage governed by the coupled inductor–capacitor relations:

$$L\frac{dI}{dt} + V_c = V_m \cos(\omega t) \tag{2}$$

$$I = C\frac{dv_c}{dt} \tag{3}$$

where L and C denote the equivalent inductance and capacitance of the network, respectively, I is the transient current, V_c is the capacitor voltage, and V_m is the peak value of the applied voltage. Solving these equations yields a high-frequency voltage rise across the interruption gap, which is essential for insulation coordination assessment.

Temporary overvoltages arise from long-line effects, load rejection, transformer energization, and ground-fault conditions [14]. The Ferranti effect causes receiving-end voltage magnification proportional to $\cosh(\gamma l)$, especially in long EHV lines. Load rejection introduces a voltage rise described by

$$V = E\frac{X_c}{X_c - X}, \tag{4}$$

where the system capacitance and generator reactance cause low-frequency temporary overvoltages. Transformer energization produces inrush and overfluxing phenomena governed by the flux relationship, which is defined as:

$$\varphi = \frac{\sqrt{2V_a}}{\omega N}(1 - \cos\omega t) + \varphi_0 \tag{5}$$

where φ is the magnetic flux in the transformer core, $V_a$is the applied phase voltage, $N$is the number of turns, $\omega$is the angular frequency, and $\varphi_0$is the residual flux prior to energization. Depending on the residual flux and core saturation characteristics, this phenomenon may sustain elevated voltage levels during the energization period.

Accurate representation of these transient behaviors requires dynamic electromagnetic modeling. The transmission line is modeled using the frequency-dependent phase-domain method, which incorporates the frequency dependence of parameters $R(\omega)$, $L(\omega)$, and $C(\omega)$, as well as traveling-wave propagation effects, making it suitable for both switching and studies of temporary overvoltages [19]. Transformer behavior is represented using mutually coupled inductances to capture saturation, inrush, and nonlinear magnetization effects. Generator sources are modeled using time-dependent sinusoidal functions with controlled start-stop intervals to reproduce transient energization dynamics. Circuit breakers are modeled as time-controlled switches that can represent random pole-closing deviations relevant to statistical switching studies. Shunt reactors are modeled using lumped R–L elements to reproduce their effect on voltage control and Ferranti mitigation.

Because the exact closing instant of each breaker pole is inherently uncertain, switching surges must be treated probabilistically. The pole-closing time is modeled as a Gaussian random variable (mean 15 ms, deviation ±15 ms), making peak SOV a stochastic outcome rather than a deterministic value. Monte Carlo Simulation is adopted, where $N = 200$ independent trials are executed. For each trial, the EMT model is solved with a randomized closing instant, producing a set of peak voltages V_i. The empirical cumulative distribution function is computed as:

$$F(v) = \frac{1}{N}\sum_{i=1}^{N}(V_i \le v) \tag{6}$$

where $F(v)$ is the probability distribution of switching overvoltages. The insulation performance is subsequently assessed using the 95th- and 98th-percentile overvoltage values in accordance with IEC 60071-2 [1]. This combined theoretical formulation of transient overvoltage mechanisms, component-level dynamic modeling, and probabilistic simulation provides the analytical foundation for evaluating the switching and temporary overvoltage performance of the 500 kV PKB–TWP interconnection.

3.2 Methodology

The overall methodology is illustrated in Fig. 2. All EMT simulations were conducted using PSCAD/EMTDC, employing the frequency-dependent phase-domain transmission line model, which has been widely validated for EHV/UHV analysis [13], [14]. The test system corresponds to the planned 500 kV PKB–TWP interconnection, which links fourteen 57 MVA, 11 kV hydro generators through fourteen 63.3 MVA, 525/11 kV step-up transformers to a 500 kV bus. Reactive power compensation was simulated using three 55 Mvar shunt reactors, while 444 kV metal-oxide surge arresters provided surge protection. The connection consists of a 120-km double-circuit line employing quad-bundle 795 MCM ACSR conductors, and the receiving end is modeled as a 500 kV infinite-bus with integrated load and shunt compensation elements [15].

To ensure consistent initialization, all cases used snapshot files derived from steady-state power flow solutions, as recommended for transient studies in PSCAD [19]. Measurement nodes were positioned at the bus, the midline section (approximately 30 kilometers), and the receiving bus to record spatial fluctuations in overvoltage.

Two primary categories of scenarios were simulated:

1) Switching overvoltages, including line energization under no-load, half-load, and full-load conditions, as well as reclosing operations following single-line-to-ground and three-line-to-ground faults.

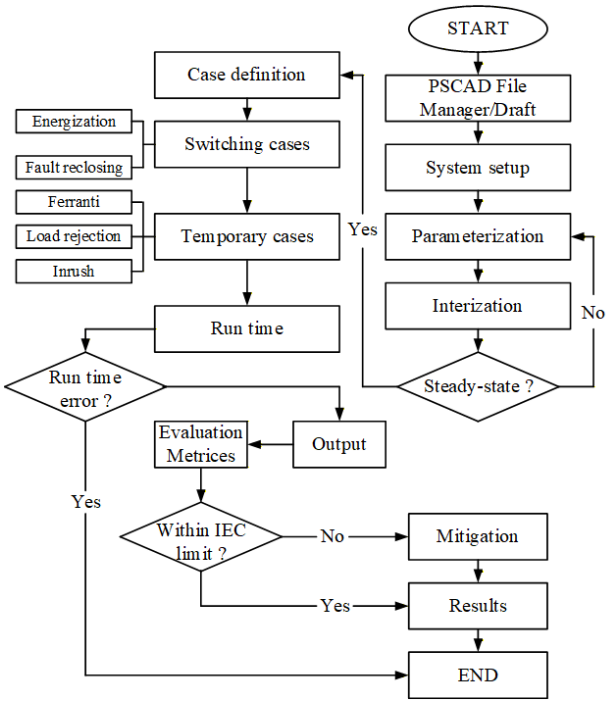

***Fig. 2**: Simulation methodology for SOV/TOV analysis in the PKB–TWP system.*

2) Temporary overvoltages—including the Ferranti effect (with and without shunt compensation), load rejection at various levels, and transformer energization with residual flux up to ±80%, consistent with field-observed inrush behavior in hydro-dominated systems [9].

To replicate real-world breaker performance, pole scatter was modeled as a Gaussian-distributed random variable with a mean closing time of 15 ms and a standard deviation of 1 ms, consistent with statistical switching studies [5]. Each scenario was simulated using 200 Monte Carlo trials to generate probability distributions of the outcomes [6]. Simulation results were analyzed using the MultiPlot interface, extracting performance indices such as peak phase-to-ground voltage (p.u.), time-to-peak, surge arrester energy absorption, and percentile statistics (95th, 98th, and maximum values). These parameters were benchmarked against the IEC 60071-2 insulation coordination limits to evaluate the adequacy of protection schemes and to identify operational condonation that requires additional mitigation [1], [8].

The simulation procedure used in this study is summarized in Fig. 2 and consists of the following steps:

1) Define all switching and temporary overvoltages operating cases, including energization, reclosing, load rejection, Ferranti effect, and transformer inrush.
2) Build a detailed EMT model in PSCAD/EMTDC using project-based parameters for generators, transformers, surge arresters, shunt reactors, and frequency-dependent transmission lines.
3) Initialize the model to steady-state to ensure realistic pre-switching conditions.
4) Apply probabilistic breaker-closing times by generating Gaussian-distributed pole-scatter values for Monte Carlo analysis.
5) Run 200 EMT simulations per case and record phase-to-ground voltage waveforms.
6) Post-process the results to extract peak values, probabilistic envelopes, and resonance locations, and compare them with IEC 60071 limits.

4. RESULTS AND DISCUSSION

This section presents EMT outcomes and interprets their implications for insulation coordination in a unified manner. Measurements were taken at the sending-end bus, the four mid-span nodes (section boundaries), and the receiving-end bus. For each case, we extract the peak phase-to-ground voltage (per-unit on the line-to-neutral basis), the peak time, and the terminal arrester energy. Statistical summaries include the mean, standard deviation, empirical percentiles (P95, P98), and maximum values. Terminology, extraction windows, and acceptance considerations follow the recognized switching-overvoltage/temporary-overvoltage practice in IEC 60071-2 [1], while modeling choices align with frequency-dependent line representations in EMT studies [13], [14].

4.1 Switching Overvoltages

Switching overvoltage arises during the energization or re-energization of high-voltage transmission lines and may exceed insulation coordination limits, particularly under no-load or light-load conditions. In this study, the 500 kV PKB–TWP double-circuit interconnection was analyzed using PSCAD/EMTDC. Several switching scenarios were considered to evaluate the transient response and to identify conditions that lead to critical overvoltage. The following subsections present results for line energization and re-energization cases.

A. Line Energization

The energization case was studied on the 500 kV PKB–TWP double-circuit transmission line. Both circuits were initially open, and only Circuit 1 was energized after the generators and transformers had reached steady state. This setup reflects practical operating conditions for assessing transient overvoltages. Fig. 3 illustrates the single-line diagram of the PKB–TWP interconnection considered in the simulations.

Fig. 4 and Fig. 5 illustrate the receiving-end voltage waveforms during line energization under different protection schemes and arrester configurations. The results show that energization transients lead to significant switching overvoltages, with peak values ranging from 1.674 p.u. to 2.251 p.u., depending on the presence of surge arresters, shunt reactors, or protection devices.

The receiving-end voltage waveforms during line energization with different protection schemes, as shown in Fig. 4(a), indicate that unmitigated energization

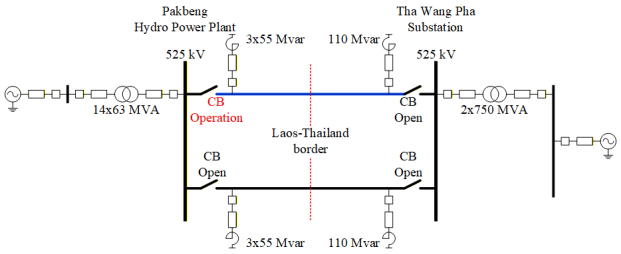

***Fig. 3**: Configuration for 500 kV line energization at PKB–TWP Circuit 1.*

produces the highest peak of 2.251 p.u. at 0.023 s, which falls within the typical switching surge range of 2.0–2.3 p.u., IEC 60071-2 [1]. The waveform exhibits a rapid transient onset followed by a damped oscillation lasting about 50 ms, characteristic of capacitive charging and traveling-wave reflections. In Fig. 4(b), the application of both 444 kV metal-oxide surge arresters and 110 Mvar shunt reactors reduces the maximum overvoltage to 1.674 p.u., representing a 25% reduction relative to the unprotected case. This illustrates the effectiveness of the coordinated protection scheme in suppressing transient surges and enhancing voltage damping. Fig. 4(c) shows that using only surge arresters without shunt compensation results in a slightly higher peak of 1.704 p.u., indicating that shunt reactors provide a complementary role by limiting line-charging currents and mitigating capacitive overvoltages. Although their contribution is less dominant than that of the arresters, the combined operation of both devices ensures that all switching surges remain within insulation coordination limits.

The receiving-end voltage waveforms with different arrester configurations are presented in Fig. 5(a). The absence of arresters at both ends produces the highest peak of 1.974 p.u. at 0.022 s, accompanied by a pronounced fast-front oscillation due to capacitive charging and traveling-wave reflections. Fig. 5(b) indicates that installing an arrester only at the PKB sending end reduces the peak to 1.685 p.u., demonstrating that the sending-end arrester effectively clamps the initial energization surge. The resulting waveform also exhibits improved damping compared with the unprotected condition. Fig. 5(c) shows that placing an arrester solely at the TWP receiving end results in a peak of 1.900 p.u., slightly higher than in the PKB-only configuration. This confirms that receiving-end protection provides only partial attenuation and is less effective in suppressing the initial fast-front surge originating near the sending end. Overall, Fig. 5 highlights the strong influence of arrester placement on switching-surge magnitudes, with sender-side protection providing the most significant reduction [6].

Overall, the PKB–TWP interconnection can experience switching surges exceeding 2.2 p.u. under uncontrolled energization. Although this value remains below the Basic Insulation Level (BIL) of 1425 kV for a 500 kV

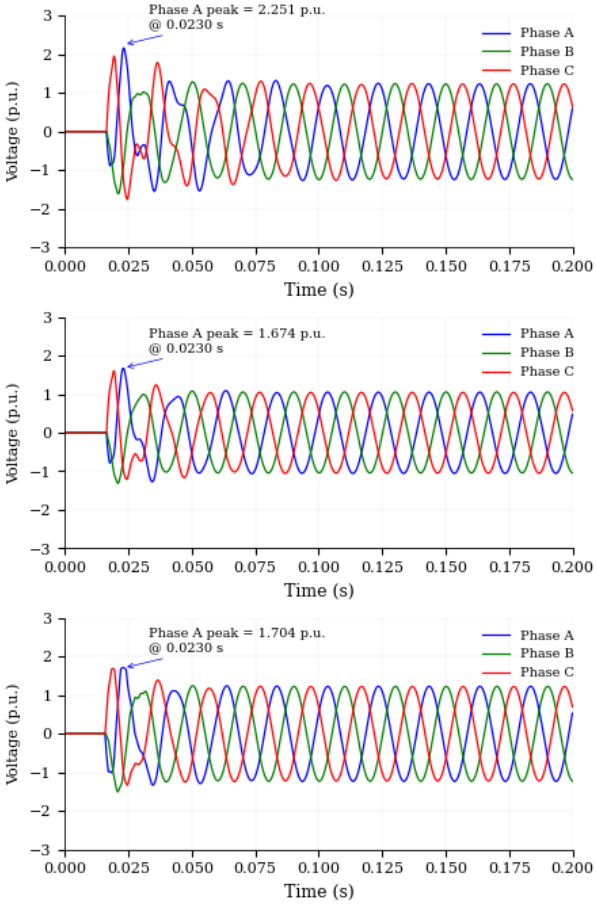

***Fig. 4**: Receiving-end voltage waveforms during line energization with different protection schemes. (a) No protection. (b) With coordinated protection. (c) Without a shunt reactor.*

system, it imposes considerable electrical and thermal stress on the surge arresters. The coordinated application of controlled switching, pre-insertion resistors, and shunt reactors can reduce these peaks by approximately 25%, thereby enhancing system reliability and reinforcing overall insulation coordination.

Table 2 summarizes the simulated switching overvoltages observed during line energization under various protection configurations. In the unprotected case, the peak voltage reached 2.251 p.u., whereas the inclusion of surge arresters and load reduced the maximum to 1.167 p.u. This substantial decrease confirms the effectiveness of the system in suppressing transient surges and enhancing insulation coordination.

B. Re-Energization after Faults.

The case of a single-line-to-ground (SLG) fault with re-energization is examined. The fault studies were conducted by varying the fault position along the line, from the sending end at PKB to the receiving end at TWP, as illustrated in Fig. 6.

Re-energization after fault clearance was simulated by applying single-line-to-ground and Three-line-to-ground

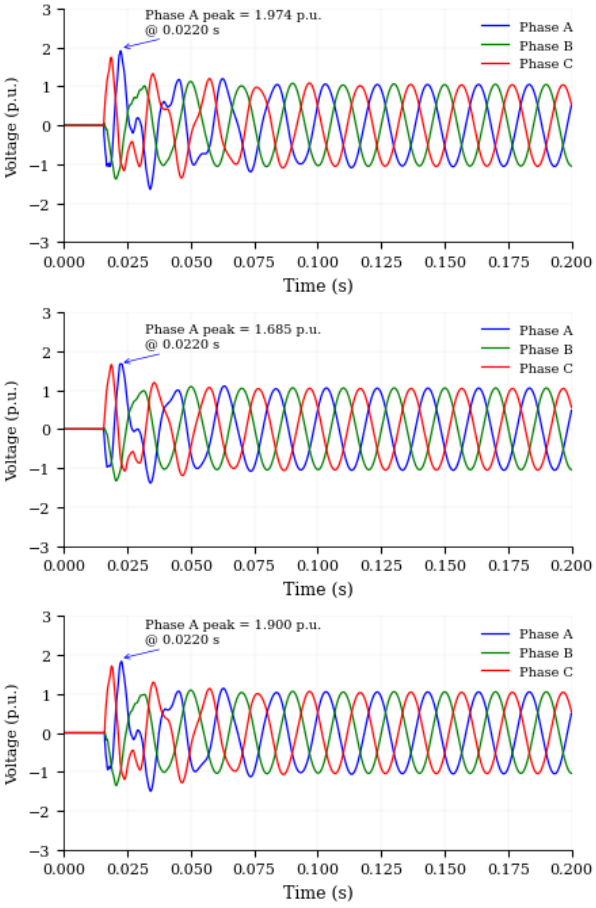

***Fig. 5**: Receiving-end voltage waveforms during line energization with different arrester configurations. (a) Without an arrester at both ends. (b) With an arrester only at PKB. (c) Arrester only at TWP.*

***Table 2**: Peak switching overvoltages during line energization (receiving end, TWP).*

Case	No-load (p.u.)	Half load (p.u.)	Full load (p.u.)	Primary Mitigation
No protection	2.251	1.425	1.119	End-point arrester installation
With protection	1.674	1.422	1.167	-
With shunt reactors	1.704	1.453	1.177	Shunt reactor re-tuning
No arrester (both)	1.974	1.460	1.178	Arresters; verify MCOV/energy
No arrester at PKB	1.685	1.334	1.152	Sending-end preference
No arrester at TWP	1.900	1.468	1.178	TWP arrester upgrade

faults at 10 ms, clearing at 50 ms, and reclosing at 100 ms. Statistical switching with 200 Gaussian-distributed

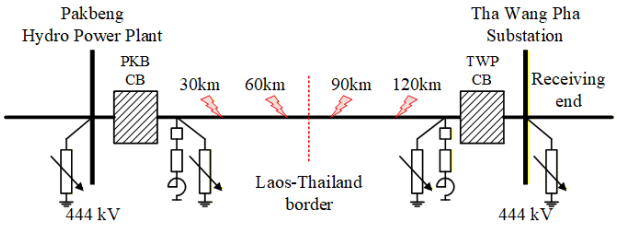

***Fig. 6**: Configuration for re-energization after a fault in the PKB–TWP transmission line.*

breaker operations (μ = 15 ms, σ = 0.5–2 ms) was used to reflect realistic breaker behavior, consistent with prior studies on stochastic switching transients [4].

In Fig. 7(a), the unprotected single-line-to-ground case produced the most severe overvoltage, reaching 3.011 p.u. at Phase B, exceeding the insulation withstand levels specified in IEC 60071-2 [1]. This steep-front surge is characteristic of traveling-wave reflections and capacitive discharge following fault clearance [13]. With full protections applied to metal-oxide surge arresters and shunt reactors, as shown in Fig. 7 (b), the single-line-to-ground peak was reduced to 1.742 p.u., demonstrating effective damping of transient surges. This result aligns with previous findings on the role of coordinated protection in limiting surge magnitudes [8]. When only surge arresters were removed, as illustrated in Fig. 7 (c), the single-line-to-ground voltage rose to 2.246 p.u., highlighting the decisive role of metal-oxide surge arresters in overvoltage limitation.

Fig. 8 shows the three-line-to-ground (3LG) re-energization waveforms under different protection configurations. In Fig. 8(a), the unprotected case produced the highest overvoltage, reaching 3.445 p.u. at Phase B, slightly higher than the single-line-to-ground scenario, and exceeding the insulation margins when complete protection metal-oxide surge arresters and shunt reactors were engaged, as shown in Fig. 8(b). The 3LG peak was limited to 1.976 p.u., demonstrating effective suppression of switching surges. However, when only surge arresters were removed, as illustrated in Fig. 8(c), the voltage rose to 2.956 p.u., confirming the critical role of coordinated surge arresters and shunt reactors in mitigating overvoltage.

The voltage waveforms observed under single-line-to-ground and three-line-to-ground conditions clearly illustrate the contrast between the sharp, high-magnitude transients in the unprotected cases and the well-damped responses achieved with coordinated protection. Table 3 summarizes these findings, confirming that single-line-to-ground re-energization without protection produces the most severe overvoltages. In contrast, the application of metal-oxide surge arresters and shunt reactors effectively limits peak values to below 1.8 p.u. Spatial monitoring along the transmission line further identified resonance hotspots approximately 60 km from the sending end, consistent with traveling-

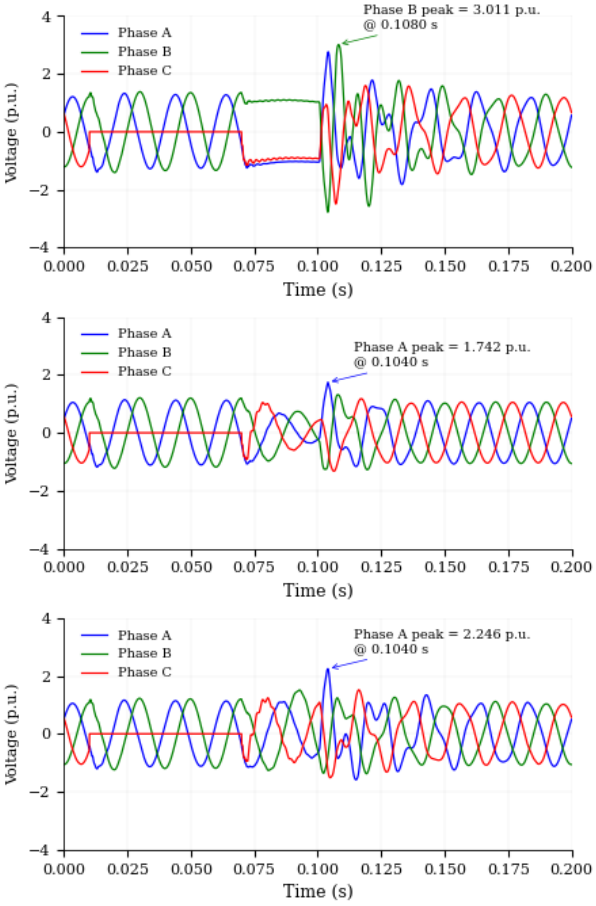

***Fig. 7**: Single-line-to-ground re-energization waveforms at the receiving end under different protection schemes. (a) No protection. (b) With coordinated protection using surge arresters and shunt reactors. (c) Without surge arresters.*

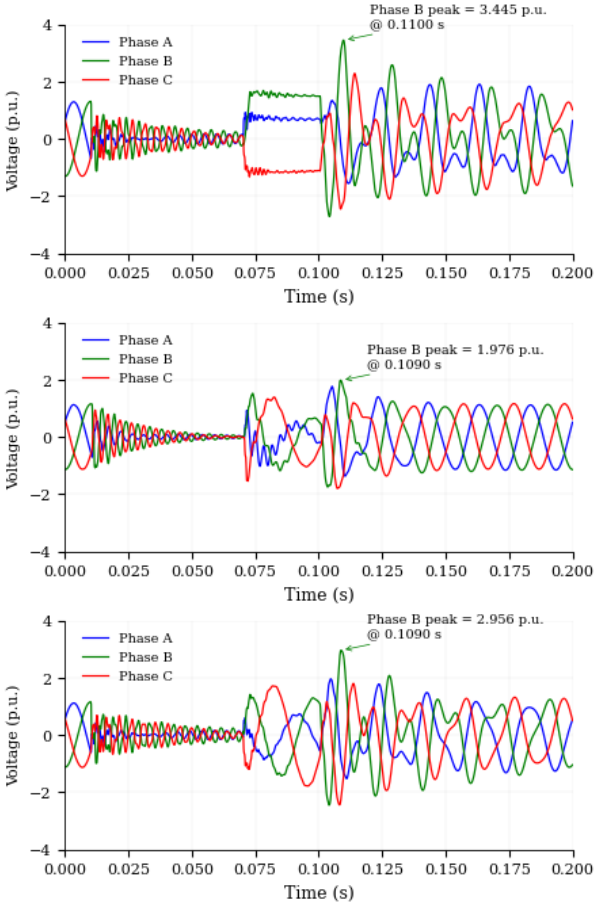

***Fig. 8**: Three-line-to-ground re-energization waveforms at the receiving end under different protection schemes. (a) No protection. (b) With coordinated protection using surge arresters and shunt reactors. (c) Without surge arrester.*

wave accumulation zones typically observed in long EHV transmission corridors [13], [14], [16].

Table 3 presents the re-energization results for both single-line-to-ground and three-line-to-ground faults. In the SLG unprotected case, the peak overvoltage reached 3.011 p.u., representing the most severe condition observed. With the coordinated application of metal-oxide surge arresters and shunt reactors, the maximum voltage was effectively limited to below 1.8 p.u. A comparable mitigation pattern was observed in the 3LG scenario, confirming the reliability of the protection scheme under various fault conditions.

4.2 Temporary Overvoltages

Temporary overvoltages were evaluated under three representative scenarios: the Ferranti effect, load rejection, and transformer inrush. These low-frequency events are critical to the steady-state and dynamic performance of long EHV lines, as they can induce voltage stresses that persist beyond fast transients [17], [18].

***Table 3**: Peak switching overvoltages during re-energization (receiving end, TWP).*

Fault Type	Protection Condition	Peak Voltage	Risk Band	Mitigation Focus
SLG	No protection	3.011 p.u.	Critical	Arresters controlled switching
SLG	With protections	1.742 p.u.	Safe / Elevated	Keep protection; verify controlled switch
SLG	No arresters (bolt)	2.246 p.u.	Critical	Restore arresters; controlled switch timing
3LG	No protection	3.445 p.u.	Critical	Arresters controlled switching
3LG	With protections	1.976 p.u.	Safe / Elevated	Maintain protection
3LG	No arresters (bolt)	2.956 p.u.	Critical	Restore arrester

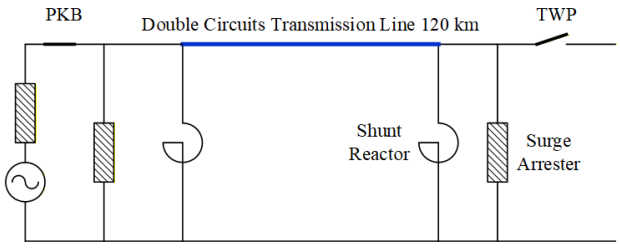

***Fig. 9**: Equivalent circuit illustrating the Ferranti effect in a 500 kV transmission line.*

A. Ferranti Effect

The Ferranti effect occurs when long transmission lines are energized under no-load or open-end conditions, resulting in a voltage rise at the receiving end due to line charging capacitance. This phenomenon is significant for 500 kV systems, where even moderate steady-state overvoltages may stress insulation or reactive compensation devices [9]. To assess this, the PKB–TWP interconnection was simulated under single- and double-circuit conditions with and without shunt reactors.

Fig. 9 shows the simplified single-line diagram of the PKB–TWP corridor considered in the Ferranti effect study. Both single- and double-circuit cases were modeled with shunt compensation applied at the terminal buses.

The study highlights that shunt reactors are essential for controlling steady-state overvoltages in lightly loaded or open-ended 500 kV lines.

Fig. 10 presents the receiving-end voltage waveforms obtained during open-end operation. With shunt reactors, the voltage was stabilized near the nominal level (0.960 p.u.) in both single- and double-circuit cases. In contrast, the absence of shunt compensation caused a rise to 1.072 p.u. for the single circuit and 1.157 p.u. for the double circuit. These results demonstrate approximately 12% and 15.7% increases in voltage, respectively, confirming the Ferranti effect. The more potent effect in the double-circuit case reflects the larger effective capacitance, while the use of reactors effectively suppressed the overvoltage to a safe level.

The results align well with both theoretical expectations and practical field observations, which typically report a 10–25% increase in voltage under open-end conditions in long EHV transmission lines [10], [11]. Table 4 further confirms that all simulated cases remain below the IEC steady-state overvoltage limit of 1.2 p.u. [1]; however, prolonged operation without shunt reactor compensation may accelerate equipment aging and compromise insulation coordination. Therefore, the inclusion of shunt compensation is validated as a critical requirement for ensuring the reliable and stable operation of the 500 kV PKB–TWP transmission corridor [7]–[9].

Table 4 indicates that although all cases remain within the IEC steady-state overvoltage limit of 1.2 p.u., pro-

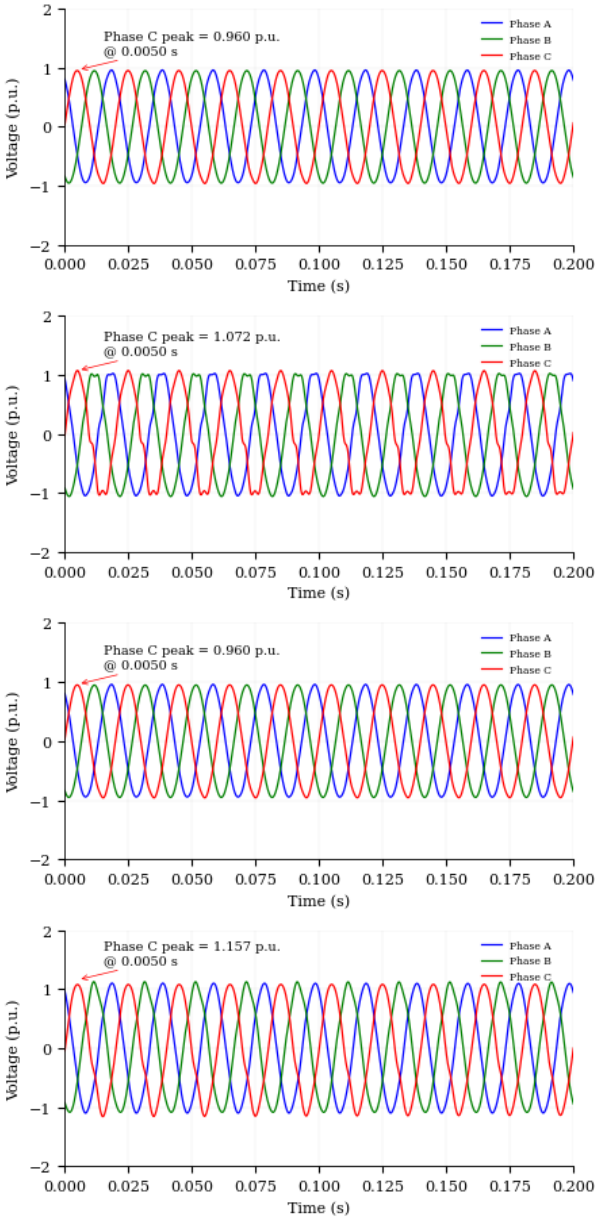

***Fig. 10**: Ferranti effect voltage waveforms at the receiving end under different operating conditions. (a) Single circuit with shunt reactors. (b) Single circuit without shunt reactors. (c) Double circuit with shunt reactors. (d) Double circuit without shunt reactors.*

longed operation without shunt reactor compensation can increase equipment stress and potentially degrade insulation performance. Consequently, the shunt compensation is confirmed to be a vital measure for ensuring reliable and stable operation of the 500 kV PKB–TWP transmission corridor.

B. Load Rejection

Load rejection causes temporary overvoltages due to the sudden removal of active and reactive power, leaving the generators supplying only the line charging current. This condition is critical for insulation coordination, as

***Table 4**: Ferranti effect results under single- and double-circuit configurations with and without reactors.*

Event	Configuration	Peak Voltage	Risk Band	Design implication
Ferranti	Single circuit, with reactors	0.960 p.u.	Safe	Normal open-end rise
Ferranti	Single circuit, no reactors	1.072 p.u.	Safe	Add reactors to trim the rise
Ferranti	Double circuit, with reactors	0.960 p.u.	Safe	Acceptable with compensation
Ferranti	Double circuit, no reactors	1.157 p.u.	Safe	Reactor sizing critical

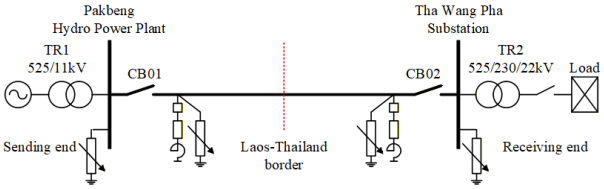

***Fig. 11**: Configuration for load rejection case in the PKB–TWP transmission line.*

it may cause a sustained voltage rise above normal operating levels. Fig. 11 illustrates the single-line configuration of the PKB–TWP system used to investigate load rejection under varying load-disconnection percentages.

Fig. 12 illustrates the voltage waveforms at node 5 for rejection levels of 30%, 60%, and 90%. In the 30% case, the maximum peak was 1.211 p.u. at 0.210 s, showing only a moderate deviation. For a 60% rejection, the peak increased to 1.270 p.u., while in the most severe 90% rejection case, the peak reached 1.317 p.u. at 0.211 s. These results confirm that higher rejection levels lead to progressively larger overvoltages, consistent with theoretical expectations that sudden removal of load produces reactive power surplus and elevated voltages.

The observed voltage magnitudes remain below the IEC steady-state temporary overvoltage limit for 500 kV systems (typically 1.4–1.5 p.u. [1]); however, the 90% load-rejection case approaches the identified critical threshold. The persistence of oscillations across multiple cycles further underscores the slow decay of temporary overvoltage phenomena relative to fast-switching surges, consistent with findings from previous EMT simulations [11], [12].

Table 5 shows that, although all cases remain technically compliant with the requirements of IEC 60071-2 [1], the 90% load-rejection scenario imposes considerable electrical stress, consistent with earlier studies [12]. These findings underscore the importance of coordinated surge arrester performance and precise generator excitation control in maintaining system stability during large-scale load rejection events.

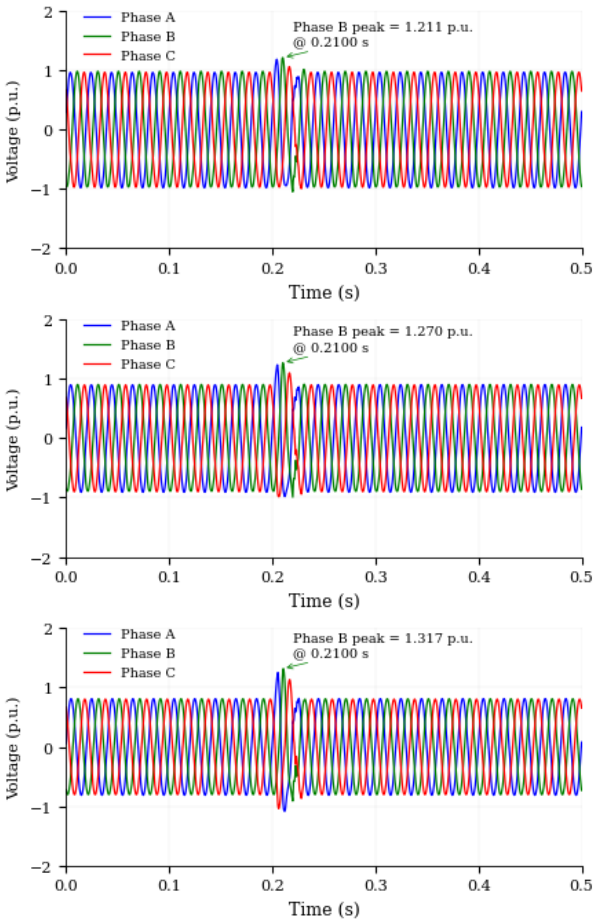

***Fig. 12**: Voltage waveforms during load rejection at node 5. (a) 30% load rejection. (b) 60% load rejection. (c) 90% load rejection.*

***Table 5**: Overvoltages under load rejection at node 5 for 30%, 60%, and 90% rejection.*

Case	Load Rejection	Peak Voltage	Time	Observation
1	30%	1.211 p.u.	0.210 s	Moderate rise, safe
2	60%	1.270 p.u.	0.210 s	Noticeable increase, within IEC limits
3	90%	1.317 p.u.	0.211 s	Highest rise, close to IEC TOV margin

C. Transformer Inrush

Transformer energization during system restoration can produce severe EMT due to residual flux and core saturation, especially in distribution-level units. These transients may distort voltage waveforms and trigger misoperation of protection relays, thereby delaying the restoration sequence. Fig. 13 illustrates the restoration topology from PKB to TWP, involving both 11 kV and 500 kV networks, and highlights the critical points where inrush phenomena are expected.

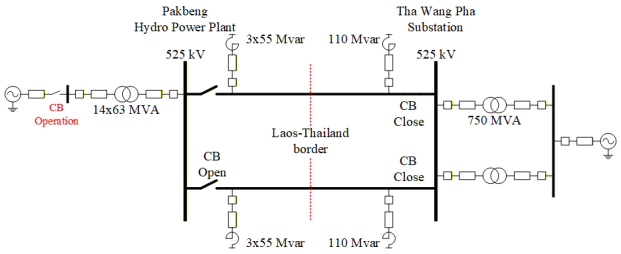

***Fig. 13**: System restoration from 11 kV and 500 kV at PKB – TWP.*

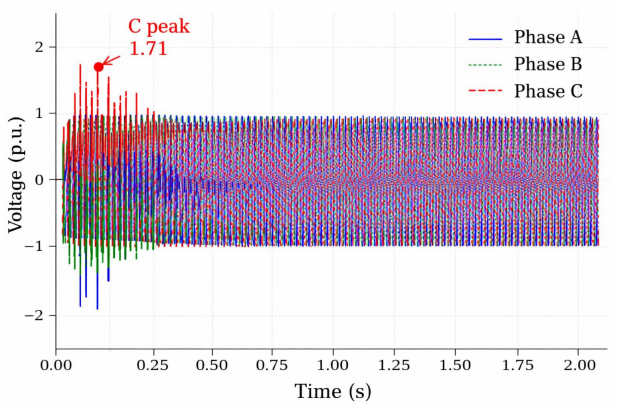

***Fig. 14**: Inrush transient during transformer energizing at PKB.*

To better understand this effect, the following results (Figs. 14–17) present inrush transient responses at the PKB and TWP substations, including voltage and current waveforms at different phases. These results offer practical insights into how transformer energization affects the stability and reliability of the overall system restoration process.

Figs. 14 and 15 present the voltage and current waveforms during energization of the 11 kV transformer at PKB. Phase C shows the highest voltage peak at 1.71 p.u. within the first 0.25 s, followed by slow damping. The inrush current reaches 34.76 A in Phase C, exhibiting significant asymmetry across phases (30.47 A in Phase A and 21.11 A in Phase B), consistent with saturation under residual flux [11]. These transients pose risks for protection relay misoperation and delayed restoration, as the distorted waveforms may trigger false fault detection. The damping time of 0.5–0.8 s further indicates prolonged stress on insulation and control systems [12].

Figs. 16 and 17 show the energization of a 525/230/22 kV autotransformer at TWP. Compared to PKB, the voltage peak is lower, with Phase B reaching 1.25 p.u. The waveform exhibits smoother recovery due to the higher transformer impedance and the controlled-energization strategy [15]. Inrush currents are minimal (2.20 A in Phase A, 2.36 A in Phase B, 0.29 A in Phase C), confirming that large autotransformers exhibit lower inrush severity [10].

The restoration topology illustrated in Fig. 13

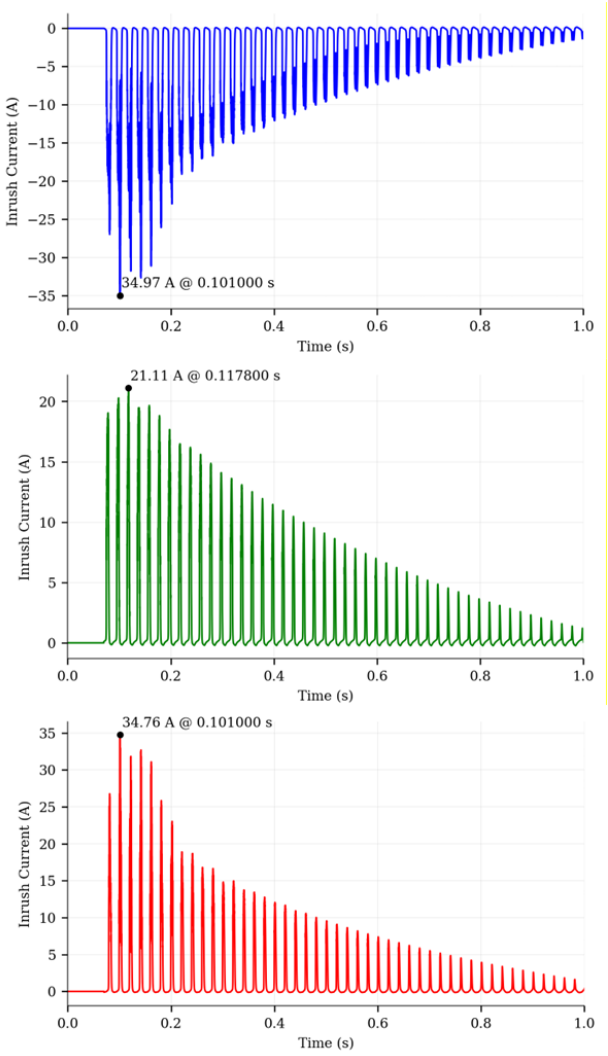

***Fig. 15**: Transformer inrush currents at PKB obtained from single-phase energization. (a) Phase A energized. (b) Phase B energized. (c) Phase C energized.*

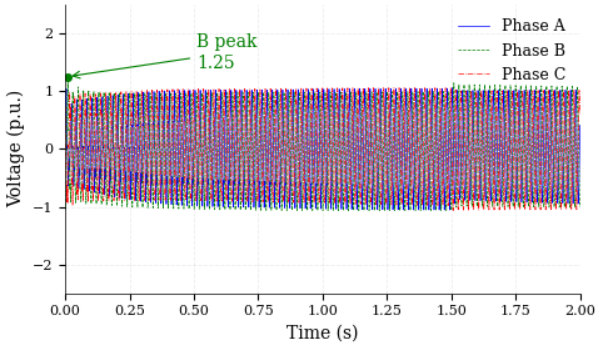

***Fig. 16**: Inrush transient during the energization of 525/230/22 kV autotransformer at TWP.*

further reinforces this principle by clearly separating the energization paths of transmission and distribution networks. Practical coordinated switching and residual flux management are therefore essential to reduce inrush

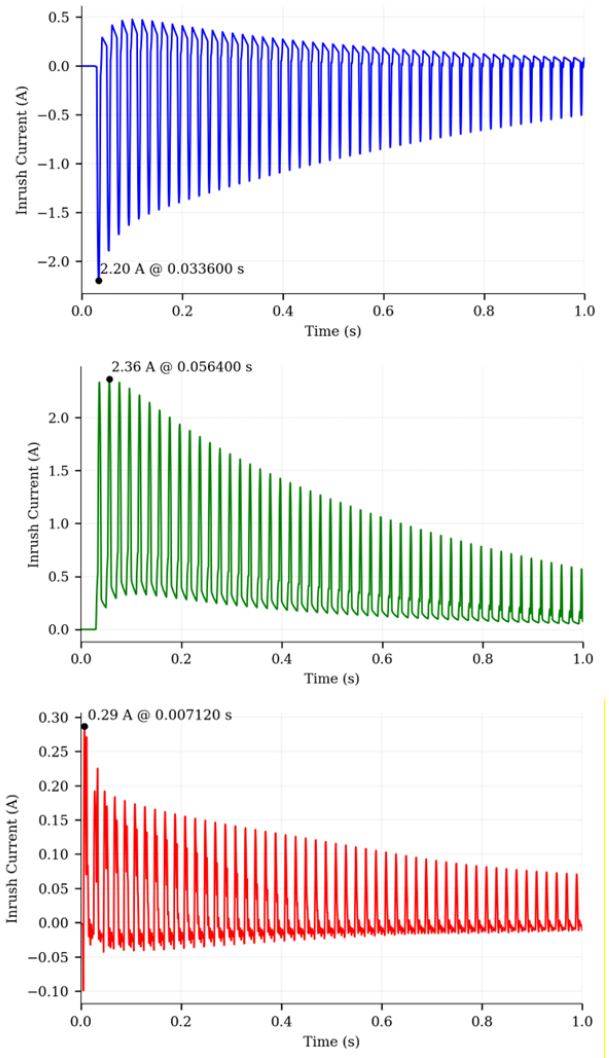

***Fig. 17**: Transformer inrush currents at TWP obtained from single-phase energization. (a) Phase A energized. (b) Phase B energized. (c) Phase C energized.*

severity and ensure a secure, reliable system restoration.

Table 6 presents the inrush characteristics observed at both substations. The PKB site exhibited markedly higher voltage and current peaks, slower damping, and greater waveform distortion, whereas TWP showed stable energization behavior with minimal transient activity. These results support the operational strategy of energizing high-voltage transmission systems before distribution-level transformers, as recommended in IEC 60071-2 [1].

5. CONCLUSION

This study provided an in-depth electromagnetic transient analysis of the 500 kV PKB–TWP interconnection between Laos and Thailand, focusing on the characterization and mitigation of switching overvoltages and temporary overvoltages using PSCAD/EMTDC. It developed a detailed frequency-dependent transmission line model and incorporated probabilistic Monte Carlo simulations to capture realistic variations in circuit breaker operation

***Table 6**: Summary of Transformer Inrush Characteristics at PKB and TWP.*

Parameter / Location	PKB 11 kV Transformer	TWP 525 kV Auto Transformer	Remarks
Peak Voltage (p.u.)	Ph-C: 1.71 p.u. (Fig. 13)	Ph-B: 1.25 p.u. (Fig. 15)	Higher overvoltage observed at PKB due to lower system strength
Peak Inrush Current (A)	Ph-A: 30.47 A, Ph-B: 21.11 A, Ph-C: 34.76 A (Fig. 14)	Ph-A: 2.20 A, Ph-B: 2.36 A, Ph-C: 0.29 A (Fig. 16)	PKB experiences much higher inrush magnitudes
Damping Behavior	Slower decay (~0.5–0.8 s)	Faster decay (<0.2 s)	Faster stabilization at TWP
Severity of Transients	High – may cause relay misoperation	Low – less risk to the protection system	The protection setting is more critical at PKB
Restoration Implication	Critical issue in distribution-level restoration	Stable energization at the transmission level	Supports energization sequence: HV before MV

and system conditions.

The results showed that uncontrolled line energization can cause switching surges up to 2.251 p.u., whereas reclosing after three-phase-to-ground faults may reach 3.445 p.u., both exceeding ≈ 2.0 p.u. insulation coordination threshold specified in IEC 60071-2. The combined use of 444-kV metal-oxide surge arresters and 110 Mvar shunt reactors effectively limited all surge magnitudes below 2.0 p.u., confirming the adequacy of the protection scheme. Temporary overvoltages caused by the Ferranti effect, load rejection, and transformer inrush stayed within acceptable limits, with maximum values of 1.157 p.u., 1.317 p.u., and 1.71 p.u., respectively. These findings suggest that the PKB–TWP transmission corridor is well compensated and operationally reliable under both transient and quasisteady conditions. Spatial monitoring along the 120-km double-circuit line identified resonance hotspots near the midline (~60 km), corresponding to traveling-wave accumulation zones. This highlights the need for distributed measurement and monitoring systems for precise insulation coordination in long EHV lines.

Overall, the study demonstrates that the 500 kV PKB–TWP interconnection fully complies with international reliability and insulation coordination standards, ensuring stable and secure power transfer between the power grids of Laos and Thailand. The probabilistic EMT-based framework established in this work enables accurate assessment of switching and temporary overvoltages under real operating conditions, supporting more efficient surge protection design and improved insulation coordination in the existing transmission network. The results provide practical technical evidence for enhancing system robustness, operational safety, and reliability of the Laos–Thailand 500 kV power corridor.

ACKNOWLEDGEMENT

The authors would like to express their sincere gratitude to Electricité du Laos (EDL) and the Electricity Generating Authority of Thailand (EGAT) for their generous financial support, which made the successful completion of this research possible. The authors also wish to extend their heartfelt appreciation to the Department of Electrical Engineering, Faculty of Engineering, Chiang Mai University, for their ongoing academic support, provision of research facilities, and invaluable technical guidance throughout this project.

REFERENCES

[1] "IEC 60071-2:2018, Insulation co-ordination—Part 2: Application guidelines," *International Electrotechnical Commission*, Geneva, Switzerland: IEC, 2018.

[2] T. Keokhoungning, S. Premrudeepreechacharn, and K.Ngamsanroaj, "Evaluation of Switching Overvoltage in 500 kV Transmission Line Interconnection Nam Theun 2 Power Plant to Roi Et 2 substation," in *2009 Asia Pacific Power and Energy Engineering Conference*, Wuhan, China, 2009, pp. 1–4.

[3] K. Ngamsanroaj and W. Tayati, "An Analysis of Switching Overvoltages in the EGAT 500 kV Transmission System," in *Proceedings of the Large Engineering Systems Conference on Power Engineering*, 2003, pp. 149-153.

[4] K. Ngamsanroaj, S. Premrudeepreechacharn, and N. R. Watson, "500 kV Single Phase Reclosing Evaluation Using Simplified Arc Model," *International Journal of Emerging Technology and Advanced Engineering*, vol. 4, no. 6, pp. 1–12, Jun. 2014.

[5] R. R. Nunes and W. do Couto Boaventura, "Insulation Coordination Considering the Switching Overvoltage Waveshape—Part I: Methodology," *IEEE Transactions on Power Delivery*, vol. 24, no. 4, pp. 2434–2440, 2009.

[6] Y. Li, J. He, J. Yuan, C. Li, J. Hu, and R. Zeng, "Failure Risk of UHV AC Transmission Line Considering the Statistical Characteristics of Switching Overvoltage Waveshape," *IEEE Transactions on Power Delivery*, vol. 28, no. 3, pp. 1731–1739, 2013.

[7] T. T. Quoc, S. L. Du, D. P. Van, N. N. Khac, L.T. Dinh, "Temporary Overvoltages in the Vietnam 500 kV Transmission line," in *1998 IEEE 8th International Conference on Transmission and Distribution Construction, Operation and Live-Line Maintenance Proceedings*, 1998.

[8] "IEC 60099-4:2014, Surge arresters—Part 4: Metal-oxide surge arresters without gaps (MOSA)," *International Electrotechnical Commission*, Geneva, Switzerland: IEC, 2014.

[9] "IEC 60099-5:2018 RLV, Surge arresters—Part 5: Selection and application recommendations," *International Electrotechnical Commission*, Geneva, Switzerland: IEC, 2018.

[10] S. A. Reddy and M. S. Kumari, "A Review of Switching Overvoltage Modeling in UHV AC Transmission Lines," *Electric Power Systems Research*, vol. 236, Nov. 2024.

[11] H. Ren, X. Wei, and H. Wu, "Influence of Line Current Limiting Reactor on Temporary Overvoltage of 500 kV Transmission Line," *Journal of Physics: Conference Series*, vol. 2592, no. 1, 2023.

[12] A. A. O. Akinrinde, A. Swanson, and I. Davidson, "Investigation and Mitigation of Temporary Overvoltage Caused by De Energization on an Offshore Wind Farm," *Energies*, 2020, 13(**??**), 4439.

[13] M. Pan, Y. Liu, and H. Zhang, "Simulation Model of UHV AC Transmission System Based on PSCAD," in *2021 International Conference on Smart Technologies and Systems for Internet of Things*, pp. 391–399, Jul. 2022.

[14] A. De Silva and D. Kothalawala, "Modelling Cables and Transmission Lines with PSCAD/EMTDC," *PSCAD Knowledge Base*, 2023.

[15] Q. Yao, Y. Liu, and Z. Wang, "Simulation and Research on Over-Voltage Suppression for High Voltage Transmission Line," *Journal of Engineering*, vol. 2018, no. 16, pp. 3060–3064, Dec. 2018.

[16] "IEEE Guide for Fault-Locating Techniques on Shielded Power Cable Systems," *IEEE Std. 1234-2019*, 2019.

[17] "IEC 60099-4: 2014, Surge arresters – Part 4: Metal-oxide surge arresters without gaps for a.c. systems," *International Electrotechnical Commission*, Geneva, Switzerland, 2014.

[18] "ABB High Voltage Products," *HS PEXLim P-T Silicone-Housed Surge Arresters – Guaranteed Protective Data*, ABB Ltd., 2019.

[19] P. Gomez, "Electromagnetic Transient Model Reconstruction of Generalized Power Transmission Lines Based on Time-Synchronized Waveform Measurements," *IEEE Access*, vol. 13, pp. 173895-173908, Oct. 2025.

[20] A. Zabihi and M. Parhamfar, "Frequency and Time Series Analysis of Surge Arrester in Power Distribution Systems," *Advances in Engineering and Intelligence Systems*, 3(**??**), pp. 94-103, Sept. 2024.

Ketsaphone Phandolak received the B.Eng. degree in Electrical Engineering from Souphanouvong University, Luang Prabang, Lao PDR. He is currently working at Electricité du Laos (EDL). His research interests include high-voltage transmission systems, switching overvoltage analysis, electromagnetic transient studies, and power system stability.

Kanchit Ngamsanroaj, B.E., M.E., and Ph.D. in Electrical Engineering, Chiang Mai University, is a senior energy systems expert with over 35 years of leadership at Thailand's Electricity Generating Authority (EGAT), where he served as Director of Operation and Maintenance for the Nam Ngum 2 Hydroelectric Power Project. His career encompasses power plant construction, grid operations, power system studies, and renewable energy integration. Currently, as a Senior Visiting Research Professor at the University of South Carolina's Hydrogen and Fuel Cell Center and an external to Chiang Mai University, he specializes in integrating hydrogen and new energy technologies into national grids. He provides strategic advisory for international hydropower collaborations and leverages his executive role in the IEEE Power and Energy Society to convert cutting-edge research into actionable insights for project viability and sustainable energy development.

Watcharin Srirattanawichaikul received the B.Eng. degree in Electrical Engineering (First Class Honors) from King Mongkut's Institute of Technology Ladkrabang, Bangkok, Thailand, in 2007, and the M.Eng. and Ph.D. degrees in Electrical Engineering from Chiang Mai University, Chiang Mai, Thailand, in 2009 and 2015, respectively. He is currently an Assistant Professor in the Department of Electrical Engineering, Faculty of Engineering, Chiang Mai University. His research interests include power electronics, power quality, microgrids, smart grids, renewable energy integration, energy storage systems and cyber-physical power systems.